Chin. Sci. Bull. (2014) 59(9):896–903
DOI 10.1007/s11434-013-0097-1

csb.scichina.com
www.springer.com/scp

Article

Atmospheric Science

Entrainment-mixing parameterization in shallow cumuli and effects of secondary mixing events

Chun-Song Lu · Yan-Gang Liu · Sheng-Jie Niu

Received: 14 May 2013 / Accepted: 19 August 2013 / Published online: 25 January 2014

Abstract Parameterization of entrainment-mixing processes in cumulus clouds is critical to improve cloud parameterization in models, but is still at its infancy. For this purpose, we have lately developed a formulation to represent a microphysical measure defined as homogeneous mixing degree in terms of a dynamical measure defined as transition scale numbers, and demonstrated the formulation with measurements from stratocumulus clouds. Here, we extend the previous work by examining data from observed cumulus clouds and find positive correlations between the homogeneous mixing degree and transition scale numbers. These results are similar to those in the stratocumulus clouds, but proved valid for the first time in observed cumulus clouds. The empirical relationships can be used to parameterize entrainment-mixing processes in two-moment microphysical schemes. Further examined are the effects of secondary mixing events on the relationships between homogeneous mixing degree and transition scale numbers with the explicit mixing parcel model. The secondary mixing events are found to be at least partially responsible for the larger scatter in the above positive correlations based on observations than that in the previous results based on numerical simulations without considering secondary mixing events.

Keywords Entrainment mixing · Cumulus · Homogeneous/inhomogeneous mixing · Observation · Model

C.-S. Lu (✉)
Key Laboratory for Aerosol-Cloud-Precipitation of China Meteorological Administration, Key Laboratory of Meteorological Disaster of Ministry of Education, Collaborative Innovation Center on Forecast and Evaluation of Meteorological Disasters, Nanjing University of Information Science and Technology (NUIST), Nanjing 210044, China
e-mail: luchunsong110@gmail.com

C.-S. Lu · Y.-G. Liu
Atmospheric Sciences Division, Brookhaven National Laboratory (BNL), Upton, NY 11973, USA

C.-S. Lu
National Key Laboratory of Numerical Modeling for Atmospheric Sciences and Geophysical Fluid Dynamics, Chinese Academy of Sciences, Beijing 100029, China

S.-J. Niu
Key Laboratory for Aerosol-Cloud-Precipitation of China Meteorological Administration, Collaborative Innovation Center on Forecast and Evaluation of Meteorological Disasters, Nanjing University of Information Science and Technology (NUIST), Nanjing 210044, China

1 Introduction

Clouds play an important role in global radiation budget [1–4]. Turbulent entrainment-mixing processes in cumulus clouds are critical to cloud–climate feedbacks, evaluation of aerosol indirect effects, and precipitation characteristics [5–10]. The above effects of entrainment-mixing processes are largely affected by different entrainment-mixing mechanisms (homogeneous or inhomogeneous), according to theoretical expectations and numerical simulations [11, 12]. In terms of observation, some suggested that the mixing mechanism was close to homogeneous, i.e., all droplets evaporate simultaneously [13]; others pointed to a nearly extreme inhomogeneous scenario, i.e., some droplets evaporate completely and others do not evaporate at all [14, 15]. Actually, entrainment-mixing processes often fall between the above two extremes [16, 17]. Motivated by such needs, Lu et al. [18] defined three new measures of

homogeneous mixing degree and examined the correlations between them and two transition scale numbers (dynamic measure for occurrence frequency of homogeneous mixing [16]). Positive correlations were found in aircraft observations of stratocumulus clouds and in numerical simulations. But currently no observational results of the correlations are reported in observed cumulus clouds. This needs to be examined in detail with in situ observations because the correlations are important for the parameterization of entrainment-mixing processes in cumulus clouds for large scale models.

Furthermore, the correlations in observed stratocumulus clouds (Fig. 2 of Lu et al. [18]) have lager scatter than those in numerical simulations (Fig. 3 of Lu et al. [18]). The scatter of the correlations in observed cumulus clouds is also expected. Although some reasons [e.g., uncertainty of adiabatic droplet number concentration (n_a)] responsible for the scatter were discussed in Lu et al. [18], secondary mixing events may be another important reason, which deserves in-depth analysis.

In this study, the correlations between the homogeneous mixing degree and transition scale numbers will be examined based on the dataset of 8 cumulus flights. Then the secondary mixing events on the scatter of the correlations will be studied with the explicit mixing parcel model (EMPM) model.

2 Correlations between homogeneous mixing degree and transition scale numbers

2.1 Microphysical measure of homogeneous mixing degree

Three measures of homogeneous mixing degree were defined in Lu et al. [18]. Due to secondary reactivation in clouds and/or the uncertainty of n_a determined from in situ observations, the first measure of homogeneous mixing degree (ψ_1) may go beyond 100 %. To account for this, ψ_1 was redefined by Lu et al. [19]

$$\psi_1 = \frac{\beta}{\pi/2}, \tag{1a}$$

$$\beta = \tan^{-1}\left(\frac{\frac{r_v^3}{r_{va}^3} - 1}{\frac{n}{n_a} - \frac{n_h}{n_a}}\right) \quad \text{for } n < n_h, \text{ or} \tag{1b}$$

$$\beta = \pi + \tan^{-1}\left(\frac{\frac{r_v^3}{r_{va}^3} - 1}{\frac{n}{n_a} - \frac{n_h}{n_a}}\right) \quad \text{for } n \geq n_h, \tag{1c}$$

where β is an angle in Fig. 1a of Lu et al. [18]; n, r_v, r_{va}, and n_h are, respectively, droplet number concentration, volume–mean radius, adiabatic volume–mean radius, and droplet number concentration during homogeneous mixing.

The second measure of homogeneous mixing degree was defined as [18]

$$\psi_2 = \frac{1}{2}\left(\frac{n - n_i}{n_h - n_i} + \frac{r_v^3 - r_{va}^3}{r_{vh}^3 - r_{va}^3}\right), \tag{2}$$

where n_i is droplet number concentration during extreme inhomogeneous mixing and r_{vh} is volume–mean radius during homogeneous mixing.

The third measure of homogeneous mixing degree (ψ_3) was defined as [18]

$$\psi_3 = \frac{\ln n - \ln n_i}{\ln n_h - \ln n_i} = \frac{\ln r_v^3 - \ln r_{va}^3}{\ln r_{vh}^3 - \ln r_{va}^3}. \tag{3}$$

2.2 Transition scale numbers

The transition scale number (N_L) is a dynamical measure of the occurrence probability of homogeneous entrainment-mixing process [16]; the larger the N_L, the stronger the homogenous entrainment-mixing process, and the weaker the inhomogeneous entrainment-mixing process. The N_L is calculated as the ratio of transition length (L^*) introduced by Lehmann et al. [17] to the Kolmogorov microscale (η)

$$N_L = \frac{L^*}{\eta} = \frac{\varepsilon^{1/2}\tau_{react}^{3/2}}{\eta}, \tag{4}$$

where ε is eddy dissipation rate; the reaction time τ_{react} is the time when droplets have completely evaporated or relative humidity has reached 99.5 % [17], whichever is first satisfied. If n_a is used in the calculation of τ_{react}, scale number is denoted by N_{La}; while if n_0 is used, scale number is denoted by N_{L0}.

2.3 RACORO data

The data used for studying the correlation between homogeneous mixing degree and transition scale number are from the RACORO field campaign, which operated over the ARM southern Great Plains (SGP) site near Lamont, Oklahoma from January 22 to June 30, 2009 [20]; "RACORO" is a short name for the routine AAF [atmospheric radiation measurement (ARM) aerial facility] clouds with low optical water depths (CLOWD) optical radiative observations field campaign. The RACORO data are downloaded from https://www.arm.gov/ for free. The data guide can be downloaded from http://www.arm.gov/publications/programdocs/doe-sc-arm-10-031.pdf, which describes the observation aircraft, instruments, principal investigators who are taking care of the data.

The dataset used here is the same as those used in Lu et al. [19]. The dataset was described in detail in Lu et al. [19] and a brief description is given here. During RACORO, comprehensive measurements of cloud, aerosol,

radiation, and atmospheric state parameters were made with the center for interdisciplinary remotely piloted aircraft studies (CIRPAS) Twin Otter aircraft. The aircraft flew at multiple levels to measure cloud droplet size distributions using the cloud and aerosol spectrometer (CAS) at a 10 Hz sampling rate. The CAS probe sizes and counts aerosol particles and cloud droplets in 20 bins from 0.29 to 25 μm (radius). Only the data with a bin-average radius larger than 1 μm are used here to calculate cloud microphysical properties [e.g., liquid–water content (LWC)]. The radius $\sim$1 μm is often taken as the lower limit of cloud droplets [21]. The cloud imaging probe (CIP) measured droplets in the range of 7.5–781 μm (radius) at a 1 Hz sampling rate. Temperature and water vapor concentration were measured at a 10 Hz sampling rate, respectively, with a Rosemount probe and the diode laser hygrometer (DLH) [22]. Dissipation rate is estimated mainly with aircraft true air speed, attack angle, and sideslip angle at a 100 Hz sampling rate using the method developed by Chan et al. [23].

Only the data collected along horizontal levels are used. The criteria for selecting clouds along these horizontal legs are as follows. Cloud droplet size distributions with LWC >0.001 g m^{-3} and $n > 10$ cm^{-3} are considered to be cloud records; use of the two criteria eliminates the measured size distributions that are contaminated by large aerosols [21]. Non-drizzling clouds must satisfy the condition that the in-cloud mean drizzle LWC (drop radius >25 μm) from the CIP over the observation period of the flight was <0.005 g m^{-3}. All the cumulus clouds analyzed here were not drizzling. One hundred and eighty-six growing cumulus clouds during eight RACORO flights are used here. As stated in Lu et al. [24], growing cumulus clouds in the eight flights were selected according to the criteria: (1) 80 % of vertical velocity in an individual cloud is positive [14, 25]; and (2) the number of cloud droplet size distributions is larger than 30 to select relatively large clouds.

The edge of the cloud core is defined as the point, going from the cloud edge toward the cloud interior, where vertical velocity varies from negative to positive for the first time (see Fig. 1a in Lu et al. [24] for details). The entrained dry air is assumed to be entrained from the air that is 500–1,000 m from the edge of a cloud core on both sides of an aircraft's cloud penetration. The reason for using this dry air is to be consistent with the two-layer scheme of cloud and environment, which has been widely used in cloud parameterizations. The average properties of this dry air are close to those from aircraft vertical soundings [24], representing the dry air far from clouds, i.e., dry air in environment. The reason for not using vertical soundings directly is that there were usually only two vertical soundings at the beginning and end of flight, so these two soundings might not represent local environments for individual clouds as well as the dry air that is 500–1,000 m from the edge of each cloud core.

To obtain the properties used in the calculations of ψ_1, ψ_2, ψ_3, $N_{\rm La}$, and $N_{\rm L0}$, mixing fraction of dry air (f) for each individual cumulus is needed and can be calculated based on Eqs. (5a–5c) [14, 17, 26]

$$q_{\rm L} + q_{\rm vs}(T) = [q_{\rm vs}(T_{\rm a}) + q_{\rm La}](1-f) + q_{\rm ve}f, \tag{5a}$$

$$c_{\rm p}T = c_{\rm p}T_{\rm a}(1-f) + c_{\rm p}T_{\rm e}f - L_{\rm v}[q_{\rm La}(1-f) - q_{\rm L}], \tag{5b}$$

$$q_{\rm vs}(T) = 0.622\frac{e_{\rm s}(T)}{p - e_{\rm s}(T)}, \tag{5c}$$

where T, $q_{\rm vs}(T)$, and $q_{\rm L}$ are, respectively, the average temperature, saturation–vapor mixing ratio, and liquid–water mixing ratio in each cumulus cloud core; $T_{\rm e}$ and $q_{\rm ve}$ are, respectively, temperature and water vapor mixing ratio in the entrained dry air; $e_{\rm s}$ is saturation–vapor pressure; $c_{\rm p}$ is specific heat capacity at constant pressure; p is air pressure; $L_{\rm v}$ is latent heat; $T_{\rm a}$, $q_{\rm vs}(T_{\rm a})$, and $q_{\rm La}$ are, respectively, the temperature, saturation–vapor mixing ratio, and liquid–water mixing ratio in the adiabatic cloud parcel. The maximum liquid–water mixing ratio in each cumulus cloud core is assumed to be $q_{\rm La}$; the temperature corresponding to $q_{\rm La}$ is assumed to be $T_{\rm a}$. Then f in each cloud core is calculated with the input parameters $q_{\rm La}$, $T_{\rm a}$, $q_{\rm L}$, $T_{\rm e}$, and $q_{\rm ve}$. The $q_{\rm La}$ is derived from adiabatic liquid–water content (LWC$_{\rm a}$), which is assumed to be the maximum LWC within a cumulus cloud core. The cloud-base height in each cloud is estimated by adiabatic extrapolation to the height of LWC$_{\rm a}$ = 0. Other methods for obtaining LWC$_{\rm a}$ and cloud-base heights were discussed in Lu et al. [19], but not workable in RACORO since cloud-base heights varied significantly during each flight in RACORO [20].

With f and assuming the maximum number concentration in each cloud is $n_{\rm a}$, $n_{\rm h}$ can be calculated with $n_{\rm h} = n_{\rm a}(1-f)$. The average number concentration in each cloud core is taken to be n. Thus, $r_{\rm v}$ is given by

$$r_v = \left(\frac{\rho_{\rm air}q_{\rm L}}{4/3\pi\rho n}\right)^{1/3}, \tag{6}$$

where ρ and $\rho_{\rm air}$ are water density and air density, respectively. Similarly, $r_{\rm va}$ is calculated with $q_{\rm La}$ and $n_{\rm a}$.

2.4 Observational correlations

With all the above properties, ψ_1, ψ_2, ψ_3, $N_{\rm La}$, and $N_{\rm L0}$ can be calculated and the results are shown in Fig. 1. The correlations between homogeneous mixing degree and transition scale numbers are positive in cumuli, consistent with the results in observed stratocumulus clouds and numerical simulations [18]. Some values of homogeneous

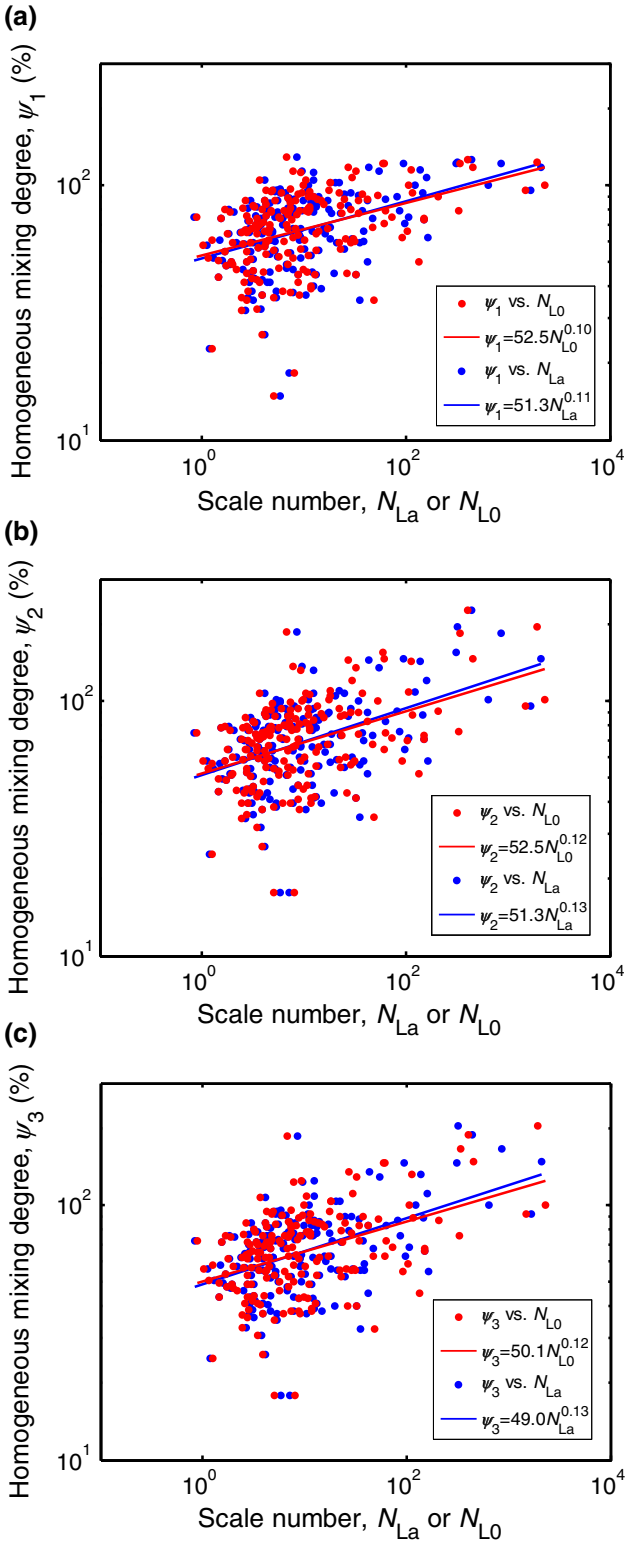

Fig. 1 Observational correlations between the three measures of homogeneous mixing degree (ψ_1, ψ_2, ψ_3) and the two scale numbers (N_{La}, N_{L0}), respectively in 186 growing cumulus clouds during RACORO

mixing degree are larger than 100 %. As explained in Lu et al. [18], this could be due to secondary reactivation in clouds or possibly due to the uncertainty of n_a determined from observations; n_a is sensitive to small scale processes, such as vertical velocity [15, 27]. Based on the correlations between homogeneous mixing degree and transition scale numbers, the entrainment-mixing processes in cumulus clouds can be parameterized in a two-moment microphysical scheme. See Lu et al. [18] for details.

Several reasons for the scatter of data points in the relationships between homogeneous mixing degree and transition scale numbers were discussed in Lu et al. [18], including dissipation rate, relative humidity, adiabatic number concentration, mixing fraction of dry air, and uncertainties of obtaining the quantities needed in Eqs. (1a, 1b, 1c–6) from observations. Another possible reason for the scatter could be secondary mixing. In the above calculations, only one entrainment-mixing process is assumed, but in reality, secondary mixing is expected to occur.

3 Effects of secondary mixing

Jensen et al. [13] studied secondary mixing with in situ observations and secondary mixing events were defined as: during a mixing event, one or both source parcels have previously participated in a primary mixing event. The secondary mixing events can be partitioned into several categories, such as mixing between two saturated, droplet-containing parcels, between a parcel with droplets, and a parcel void of droplets. Here "secondary mixing" means the dry air blobs are entrained one at a time instead of all at the same time.

The EMPM model, developed by Krueger et al. [28], is used to study secondary mixing. Su et al. [29] further included individual droplet growth in the model. The model depicts the fine-scale internal structure of a rising parcel using a 1D domain. The internal structure evolves in the model as a consequence of discrete entrainment events and explicit turbulent mixing based on the linear eddy model developed by Kerstein [30]. The model works as follows. First, the parcel ascends adiabatically above cloud-base and the droplets grow by condensation. Second, when entrainment occurs, the entrained dry air replaces a same-sized segment of the cloudy parcel. Third, the cloudy air and the entrained dry air undergo a finite rate turbulent isobaric mixing process, during which many droplets encounter the entrained dry air, resulting in partial or even total evaporation.

The cloud-base and environmental information are taken from 186 growing clouds analyzed above. The average

cloud-base pressure, temperature, and water vapor mixing ratio of these clouds are 812.7 hPa, 287.1 K, and 12.4 g kg^{-1}, respectively. The average n_a is 1,107 cm^{-3}, which is too large for the EMPM model. Here n_a is set to be 500 cm^{-3} and these droplets are randomly assigned to the 20 m (width) × 0.001 m (height) × 0.001 m (depth) model domain. The effect of the arbitrary n_a will be discussed later. The average height of aircraft observation levels above cloud bases is taken as the entrainment level, where the average pressure is 798.6 hPa, the temperature and water vapor mixing ratio in the entrained air are 286.8 K and 10.4 g kg^{-1}, respectively. The average ε is 5.7e^{-3} m^2 s^{-3}. Updraft is set to be a constant, 2 m s^{-1}, before the entrainment level; after that the parcel stops rising and isobaric mixing occurs. The grid size is set to be 0.0017 × 0.001 × 0.001 m^3. The time step of model output is 0.75 s.

Entrainment-mixing processes are random in terms of entrained dry air blob size and time interval between two entrainment events [31]. The entrained dry air blob size is set according to the cumulus observations in RACORO. The probability density (y) of mixing fraction of dry air in the 186 growing cumulus clouds follows a log normal distribution (Fig. 2),

$$y = \frac{1}{f\sigma\sqrt{2\pi}} e^{-(\ln f-\mu)^2/2\sigma^2}, \tag{7}$$

where the average ln(f) is $\mu = -2.5$, and the standard deviation of ln(f) is $\sigma = 0.62$. A group of f is randomly produced according to Eq. (7). Assuming that it takes q times to entrain the dry air into the model domain, then the dry air blob entrained each time is,

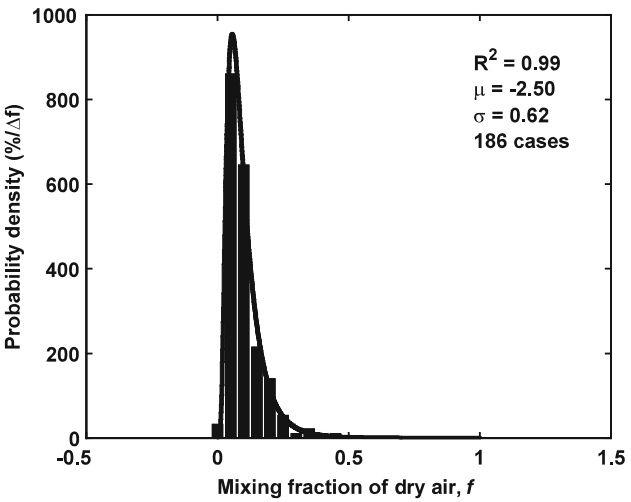

Fig. 2 Probability density function of mixing fraction of dry air (f) in 186 growing cumulus clouds during RACORO. The f bin width (Δf) for the PDF is 0.05. Also provided are the coefficient of determination (R^2), the mean (μ) and standard deviation (σ) of ln(f) and a *red line* of the lognormal fit

$$f_q = f/q \times 20 \times 0.001 \times 0.001 \text{ m}^3. \tag{8}$$

The time interval between two entrainment events is determined assuming entrainment mixing is a Poisson process [28], and the probability distribution of the time interval between mixing events can be described by,

$$P = 1 - e^{-t/t_m}, \tag{9}$$

where t_m is average time interval. During simulations, q is set to be 4, 6, 8, 10, and t_m is set to be 0, 1, 2, 4, 6, 8, 10, 12, 14, 16, 18, and 20 s. During entrainment-mixing processes, liquid–water mixing ratio decreases. It is assumed that new saturation is achieved when the liquid–water mixing ratio stops decreasing for a 5-s period; the n and r_v in the model domain are taken as the final values used in the calculations of ψ_1, ψ_2, and ψ_3. Sensitivity tests show that the values of ψ_1, ψ_2, and ψ_3 are not sensitive to the waiting period of "5 s" [18].

Figure 3 shows the three measures of homogeneous mixing degree as a function of t_m for different q. The lines for ψ_2 and ψ_3 are almost overlapped. The three measures of homogeneous mixing degree have the largest values for $t_m = 0$ s, i.e., all dry air blobs are entrained into the cloud simultaneously without secondary mixing events. When $t_m = 0$ s, the initial droplets during mixing have adiabatic droplet sizes. When $t_m > 0$ s, secondary mixing occurs and the initial droplets in these mixing events are smaller than those in the adiabatic cloud because of previous mixing events. The smaller droplet sizes, the faster evaporation. Therefore, the mixing mechanism tends to be more inhomogeneous (smaller homogeneous mixing degree) for $t_m > 0$ s than for $t_m = 0$ s. The average deviations of ψ_1 for $t_m > 0$ s from those for $t_m = 0$ s are −12.6 %, −10.3 %, −8.5 %, and −9.5 % for $q = 4$, 6, 8, and 10, respectively. The average deviations of ψ_2 for $t_m > 0$ s from those for $t_m = 0$ s are −14.7 %, −12.3 %, −10.6 %, and −11.0 % for $q = 4$, 6, 8, and 10, respectively; ψ_3 is close to ψ_2.

The homogeneous mixing degree varies with increasing t_m when $t_m > 0$ s, but there is no clear trend. In addition to t_m, the homogeneous mixing degree also depends on q (Fig. 3). In each growing cumulus cloud during RACORO, t_m and q may be both different. The combination of the effects of t_m and q causes different deviation of homogeneous mixing degree for different clouds. The transition scale numbers are not affected by secondary mixing events because the quantities needed in the calculations are independent of secondary mixing events. So even for the same transition scale number, the homogeneous mixing degree varies due to secondary mixing events and partially causes the scatter of the data points in Fig. 1. Figure 3 of Lu et al. [18] showed the correlations between homogeneous mixing degree and transition scale numbers based on EMPM simulations, which were not affected by

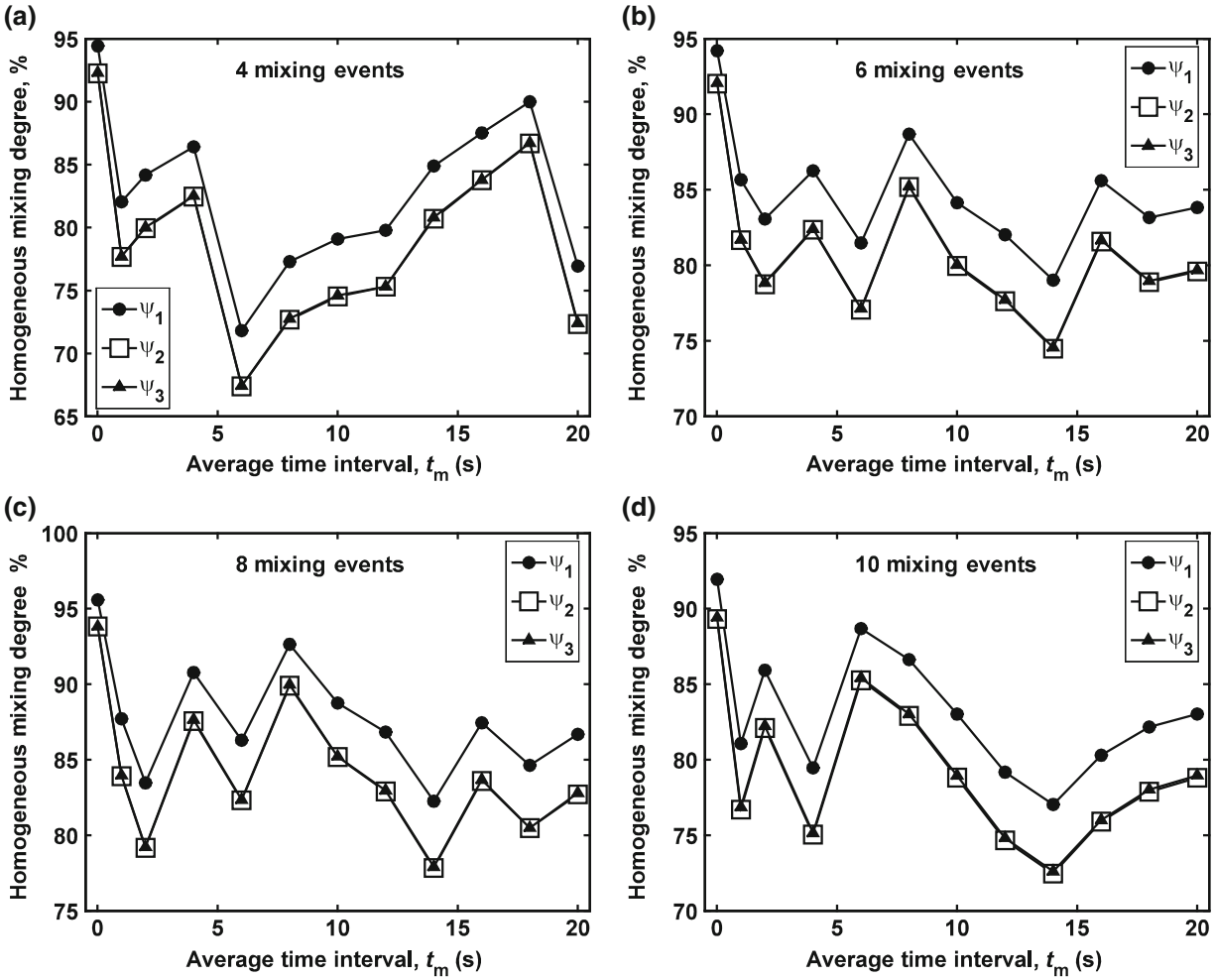

Fig. 3 Homogeneous mixing degree ($\psi 1$, $\psi 2$, $\psi 3$) as a function of average time interval between mixing events (t_m) based on numerical simulations by the Explicit Mixing Parcel Model (EMPM). **a** Four mixing events, **b** six mixing events, **c** eight mixing events, and **d** ten mixing events are assumed

secondary mixing. The data points in Fig. 3 of Lu et al. [18] have smaller scatter than those in Fig. 1 in this study, where secondary mixing events are expected to occur. To fully understand the scatter in Fig. 1, secondary mixing events and also the factors investigated in Lu et al. [18] should all be considered; these factors include dissipation rate, relative humidity, adiabatic number concentration, mixing fraction of dry air, and observational uncertainties of the quantities used in the calculation of homogeneous mixing degree and transition scale numbers.

In addition, the values of ψ_1, ψ_2, and ψ_3 for both $t_m > 0$ s and $t_m = 0$ s would all decrease if n_a was set to be 1,007 cm^{-3} instead of 500 cm^{-3}. The reason is that a larger n_a causes smaller droplets, increasing the likelihoods of complete evaporation and extreme inhomogeneous mixing [32]. It is noteworthy that aerosol affects cloud microphysical properties (e.g., n_a) and entrainment-mixing mechanisms [33–35], thus it is necessary to account for aerosol in the future study based on observations and numerical simulations with spectral bin microphysics schemes [36, 37] or double-moment bulk microphysics schemes [38].

4 Concluding remarks

Three microphysical measures of homogeneous mixing degree are found all positively correlated with transition scale numbers in growing cumuli observed during the RACORO field campaign. The transition scale numbers are used to indicate the probability of occurrence of homogeneous mixing processes. The positive correlations are found valid in cumulus clouds based on observations for the first time. These correlations can be used to parameterize entrainment mixing in cumulus clouds for large scale models.

The effects of secondary mixing (i.e., the dry air blobs are entrained one at a time instead of all at the same time) on the scatter in the above relationships are examined with the EMPM. The mixing fraction of dry air entrained into the model domain is assumed to follow a log normal distribution based on RACORO observations. The time interval between secondary mixing events follows an exponential distribution assuming entrainment mixing is a Poisson process. Generally, homogeneous mixing degree decreases for secondary mixing events (time interval >0) compared with that for only one primary mixing event (time interval $= 0$), because the initial droplets in secondary mixing events are smaller than those in the adiabatic cloud. For each cloud, the decrease of homogeneous mixing degree depends on both the mean time interval and the number of secondary mixing events. Such effects of secondary mixing events are partially responsible for the scatter of data points in the correlations between homogeneous mixing degree and transition scale numbers.

Acknowledgments This research was supported by the National Natural Science Foundation of China (41030962, 41305120, 41375138, 41275151, 41075029, 41375137, 41305034); the Natural Science Foundation of Jiangsu Province, China (BK20130988, BK2012860); the Specialized Research Fund for the Doctoral Program of Higher Education (20133228120002); the Natural Science Foundation of the Higher Education Institutions of Jiangsu Province, China (13KJB170014); China Meteorological Administration Special Public Welfare Research Fund (GYHY201406007); the Open Funding from National Key Laboratory of Numerical Modeling for Atmospheric Sciences and Geophysical Fluid Dynamics; the Open Funding from Key Laboratory for Aerosol-Cloud-Precipitation of China Meteorological Administration, China (KDW1102, KDW1104, KDW1201); the Open Funding from Key Laboratory of Meteorological Disaster of Ministry of Education, China (KLME1305, KLME1205, KLME1107); the Qing-Lan Project for Cloud-Fog-Precipitation-Aerosol Study in Jiangsu Province, China; a Project Funded by the Priority Academic Program Development of Jiangsu Higher Education Institutions; the U.S. Department of Energy's (DOE) Earth System Modeling (ESM) program via the FASTER project (www.bnl.gov/faster) and Atmospheric System Research (ASR) program. We appreciate the helpful discussions about the RACORO data with Andrew Vogelmann, Haf Jonsson, Greg McFarquhar, Glenn Diskin, Gunnar Senum and Hee-Jung Yang. We also thank Steven Krueger and Timothy Wagner for their help with the EMPM model.

References

1. Zhang H, Peng J, Jing X et al (2013) The features of cloud overlapping in Eastern Asia and their effect on cloud radiative forcing. Sci China Earth Sci 56:737–747
2. Jing X, Zhang H, Guo P (2009) A study of the effect of sub-grid cloud structure on global radiation in climate models. Acta Meteorol Sin 67:1058–1068 (in Chinese)
3. Nie J, Kuang Z (2012) Responses of shallow cumulus convection to large-scale temperature and moisture perturbations: a comparison of large-eddy simulations and a convective parameterization based on stochastically entraining parcels. J Atmos Sci 69:1936–1956
4. Song X, Zhang G, Li J (2012) Evaluation of microphysics parameterization for convective clouds in the NCAR Community atmosphere model CAM5. J Clim 25:8568–8590
5. Yum S (1998) Cloud droplet spectral broadening in warm clouds: an observational and model study. Dissertation, University of Nevada
6. Kim BG, Miller MA, Schwartz SE et al (2008) The role of adiabaticity in the aerosol first indirect effect. J Geophys Res 113:D05210
7. Del Genio AD, Wu J (2010) The role of entrainment in the diurnal cycle of continental convection. J Clim 23:2722–2738
8. Liu Y, Daum PH, Chai SK et al (2002) Cloud parameterizations, cloud physics, and their connections: an overview. Recent Res Dev Geophys 4:119–142
9. Lu C, Liu Y, Niu S (2013) A method for distinguishing and linking turbulent entrainment mixing and collision-coalescence in stratocumulus clouds. Chin Sci Bull 58:545–551
10. Lin Y, Zhao M, Ming Y et al (2013) Precipitation partitioning, tropical clouds, and intraseasonal variability in GFDL AM2. J Clim 26:5453–5466
11. Baker MB, Breidenthal RE, Choularton TW et al (1984) The effects of turbulent mixing in clouds. J Atmos Sci 41:299–304
12. Chosson F, Brenguier JL, Schüller L (2007) Entrainment-mixing and radiative transfer simulation in boundary layer clouds. J Atmos Sci 64:2670–2682
13. Jensen JB, Austin PH, Baker MB et al (1985) Turbulent mixing, spectral evolution and dynamics in a warm cumulus cloud. J Atmos Sci 42:173–192
14. Gerber HE, Frick GM, Jensen JB et al (2008) Entrainment, mixing, and microphysics in trade-wind cumulus. J Meteorol Soc Jpn 86A:87–106
15. Freud E, Rosenfeld D, Kulkarni JR (2011) Resolving both entrainment-mixing and number of activated CCN in deep convective clouds. Atmos Chem Phys 11:12887–12900
16. Lu C, Liu Y, Niu S (2011) Examination of turbulent entrainment-mixing mechanisms using a combined approach. J Geophys Res 116:D20207
17. Lehmann K, Siebert H, Shaw RA (2009) Homogeneous and inhomogeneous mixing in cumulus clouds: dependence on local turbulence structure. J Atmos Sci 66:3641–3659
18. Lu C, Liu Y, Niu S et al (2013) Exploring parameterization for turbulent entrainment-mixing processes in clouds. J Geophys Res 118:185–194
19. Lu C, Liu Y, Niu S et al (2013) Empirical relationship between entrainment rate and microphysics in cumulus clouds. Geophys Res Lett 40:2333–2338
20. Vogelmann AM, McFarquhar GM, Ogren JA et al (2012) RACORO extended-term aircraft observations of boundary layer clouds. Bull Am Meteorol Soc 93:861–878
21. Deng Z, Zhao C, Zhang Q et al (2009) Statistical analysis of microphysical properties and the parameterization of effective radius of warm clouds in Beijing area. Atmos Res 93:888–896
22. Diskin GS, Podolske JR, Sachse GW et al (2002) Open-path airborne tunable diode laser hygrometer. Proc SPIE 4817:196–204
23. Chan KR, Dean-Day J, Bowen SW et al (1998) Turbulence measurements by the DC-8 meteorological measurement system. Geophys Res Lett 25:1355–1358
24. Lu C, Liu Y, Niu S et al (2012) Lateral entrainment rate in shallow cumuli: dependence on dry air sources and probability density functions. Geophys Res Lett 39:L20812
25. Lu C, Liu Y, Yum S et al (2012) A new approach for estimating entrainment rate in cumulus clouds. Geophys Res Lett 39:L04802
26. Burnet F, Brenguier JL (2007) Observational study of the entrainment-mixing process in warm convective clouds. J Atmos Sci 64:1995–2011

27. Lu C, Liu Y, Niu S et al (2012) Observed impacts of vertical velocity on cloud microphysics and implications for aerosol indirect effects. Geophys Res Lett 39:L21808
28. Krueger S, Su C, McMurtry P (1997) Modeling entrainment and finescale mixing in cumulus clouds. J Atmos Sci 54:2697–2712
29. Su CW, Krueger SK, McMurtry PA et al (1998) Linear eddy modeling of droplet spectral evolution during entrainment and mixing in cumulus clouds. Atmos Res 47–48:41–58
30. Kerstein AR (1988) A linear-eddy model of turbulent scalar transport and mixing. Combust Sci Technol 60:391–421
31. Romps DM, Kuang Z (2010) Nature versus nurture in shallow convection. J Atmos Sci 67:1655–1666
32. Hill AA, Feingold G, Jiang H (2009) The influence of entrainment and mixing assumption on aerosol–cloud interactions in marine stratocumulus. J Atmos Sci 66:1450–1464
33. Yu X, Dai J, Lei H et al (2005) Physical effect of cloud seeding revealed by NOAA satellite imagery. Chin Sci Bull 50:44–51
34. Lu GX, Guo XL (2012) Distribution and origin of aerosol and its transform relationship with CCN derived from the spring multi-aircraft measurements of Beijing cloud experiment (BCE). Chin Sci Bull 57:2460–2469
35. Xue H, Feingold G, Stevens B (2008) Aerosol effects on clouds, precipitation, and the organization of shallow cumulus convection. J Atmos Sci 65:392–406
36. Liu X, Niu S (2009) Numerical simulation on the evolution of cloud particles in 3-D convective cloud. Ser D:Earth Sci 52:1195–1206
37. Yin Y, Chen Q, Jin L et al (2012) The effects of deep convection on the concentration and size distribution of aerosol particles within the upper troposphere: a case study. J Geophys Res 117:D22202
38. Chen B, Yin Y (2011) Modeling the impact of aerosols on tropical overshooting thunderstorms and stratospheric water vapor. J Geophys Res 116:D19203